Supporting Information

Zou et al. 10.1073/pnas.1216913110

SI Methods

Animals. Generation of TRE-*Sod3*-GFP transgenic (1) and extracellular-superoxide dismutase (EC-SOD) knockout mice (*Sod3*$^{-/-}$) (2) has been described; CamKII-tTA transgenic mice (3) were initially obtained from the Jackson Laboratory (stock no. 007004). All three mouse strains were maintained on the C57BL/6J background. To generate TRE-*Sod3*-GFP and CamKII-tTA double-transgenic mice on the EC-SOD–null background, each transgenic line was crossed to EC-SOD KO in two successive rounds of breeding to generate TRE-*Sod3*-GFP/KO and CamKII-tTA/KO mice. The absence of endogenous EC-SOD protein in TRE-*Sod3*-GFP/KO and CamKII-tTA/KO mice was verified by Western blot analysis of mouse serum (1). Crosses between TRE-*Sod3*-GFP/KO and CamKII-tTA/KO mice generated TRE-*Sod3*-GFP/CamKII-tTA double-transgenic mice on the EC-SOD null background and the mice were designated as overexpressors (OE) in this study. EC-SOD knockout mice were generated from the same breeding as littermates and were designated as KO. Because the breeding could not provide WT controls, C57BL/6J mice were generated in parallel in the same housing area and were designated as WT. All mice were kept in a barrier facility with a 12-h dark-light cycle, given food and water ad libitum, and maintained in microisolators with a constant temperature between 20 °C and 26 °C. All animal procedures were reviewed and approved by the Subcommittee on Animal Studies (National Institutes of Health assurance number A3088-01) at the Veteran's Affairs Palo Alto Health Care System and in accordance with the Public Health Service Policy on Humane Care and Use of Laboratory Animals.

All transgenic and KO mice were identified by PCR genotyping. TRE-*Sod3*-GFP and CamKII-tTA mice were genotyped as previously described (1) and EC-SOD KO mice were genotyped with the following primers: (forward) 5′-GTT TCC ACC CAA TGT CGA GC-3′ and (reverse) 5′-CCA GTC ATA GCC GAA TAG CC-3′ primers for the KO allele; (forward) 5′-GCA ATC TGC AGG GTA CAA CC-3′ and (reverse) 5′-TCT TGC GCT CCT TTG TCT GG-3′ primers for the WT allele. PCR products for the WT and KO allele were ∼500 bp and 300 bp, respectively. Because of the high GC content in EC-SOD sequence, 40% (vol/vol) DMSO was included in the 10× PCR buffer [200 mM Tris, PH 9.0, 160 mM $(NH_4)_2SO_4$] and the reaction was carried out for 35 cycles (94 °C for 30 s, 60 °C for 30 s, and 72 °C for 30 s).

Cranial Irradiation. Two-mo-old male WT, KO, and OE mice were anesthetized (intraperitoneal injection, 120 mg/kg ketamine, and 5 mg/kg xylazine) and sham-irradiated or irradiated with a single dose of 5 Gy using a Mark 1 Cesium Irradiator (J. L. Shepherd and Associates) with an dose rate of 71.4 cGy/min. Details of irradiation set up has been described previously (4, 5), with the mouse body shielded with a minimum of 5-cm lead in all directions and the head exposed to the source of the irradiator through the opening of the lead shield. Radiation dose was monitored by placing the InLight nanoDot (Landauer) dosimeter in the mouse holder at the location of the mouse head.

Behavioral Tests. Before the behavioral tests, each mouse was habituated to handling by laboratory personnel for 1–2 min each day for 7 d. All behavioral studies were captured by a digital camera and the study results analyzed by TopScan Lite (Cleversys) or by hand. Each experimental group included 17–20 animals. All animals received sham or cranial irradiation at 2 mo of age, and behavior studies were commenced 1 mo following irradiation (Fig. 1*A*). Behavioral tests were carried out in the following order: open field, novel location recognition (NLR) and novel object recognition (NOR), elevated zero maze, and radial-arm water maze (RAWM). A separate set of mice were used for the assessment of tactile and heat sensitivities.

Open field. The open-field arenas were constructed with white opaque high-density polyethylene plastic and each measured 45 × 45 × 45 cm. The entire box was wiped with 70% (vol/vol) alcohol between each test subject. Each mouse was placed into the arena from the middle of the south wall under dim light and allowed to explore the box for 10 min. Overall activities and the time spent in the center vs. the outer 50% area were determined for each mouse. The time spent in the center 50% area was used as an index of general anxiety levels.

Novel location and novel object recognition. NLR and NOR tasks were carried out in the same arenas as that used for the open field test. A large visual cue was placed on the north wall of the arena, and mice were always placed into the arena from the middle of the south wall. One day after the open field test, each mouse was left in the arena with two identical objects (OBJ1 and OBJ2, made of Lego blocks) for 10 min for habituation. The two identical objects were placed side by side with equal distance from the east and west walls and were 30 cm away from the visual cue (i.e., the north wall). The next day, mice were first given three 10-min trials with identical setting from the day before. The time spent exploring the two objects was recorded. In the fourth 10-min trial, OBJ1 was moved toward the visual cue (novel location), and the time spent exploring OBJ1 in the new location was recorded. In the fifth 10-min trail, OBJ2 (the familiar object) was replaced by a new object of different shape and color (OBJ3, novel object), and the time spent exploring OBJ3 was recorded. The intertrial intervals were 5 min and mice were returned to their home cage during that time. Objects were replaced with replicates after each trial, and 4% (vol/vol) acetic acid was used to clean and remove potential odors. Exploration behavior in the first 5 min was used to assess location (trial 4) and object (trial 5) recognition. The data were calculated as exploration ratio for and as time (in seconds) spent exploring OBJ1 in the novel location (in trial 4) vs. that for exploring OBJ2 in its original location (in trial 4) in NLR. Exploration ratio for and time spent exploring the novel object (OBJ3) vs. that for exploring the familiar object (OBJ1) in trial 5 were calculated for novel object recognition. Exploration ratio for novel and familiar location/object was calculated as *T*novel/(*T*novel + *T*familiar) and *T*familiar/(*T*novel + *T*familiar), respectively, where *T* equals time, as previously described (6).

Elevated zero maze. The elevated zero maze was constructed based on a published design (7) with an outer diameter of 24 inches and inner diameter of 20 inches, and sits 24 inches above the floor. Walls in the closed quadrants are 6 inches tall. Mice were placed facing the closed quadrant 1 of the elevated zero maze to begin the 5-min test period. The latency to enter an open quadrant, total time spent in open and closed quadrants, time in each of the four quadrants, and the activity in closed quadrants were recorded. Distance traveled and the number of fecal boli at the end of each test was also calculated. Several of these measurements were used to determine general anxiety. After mice were tested, the chamber was cleaned with 70% ethanol and allowed to dry.

Radial-arm water maze. RAWM is a hippocampus-dependent task that has been described at length in previous publications (8, 9). Mice received a total of 15 trials on each of the training and test day, including two 30-min breaks following trials 6 and 12. During the break period, the mice were returned to their home cages. On the first day (training day), trials 1–12 alternated between visible and hidden platforms, and trials 13–15 used hidden platform only.

On the second day (test day), mice were given 15 trials of hidden-platform test in the RAWM to assess their memory for the hidden-platform location. Spatial learning and memory was measured by counting the number of arm entry errors that mice made on each trial. An arm entry error was operationally defined as entering one of the arms that did not contain either the visible or the hidden platform. Average arm entry errors were calculated for blocks of three trials.

Tactile sensitivity. Tactile sensitivity was measured by using von Frey filaments following the "up-down" method described by Chaplan et al. (10), Sahbaie et al. (11), and DeLorey et al. (12). After acclimating mice on wire mesh platforms inside clear cylindrical plastic enclosures (10-cm diameter, 40-cm height), fibers of sequentially increasing stiffness were applied to the plantar aspect of the hind paw. The fiber was pressed and left in place for 5 s, and hind paw withdrawal was scored as a response. After the initial response, four fibers were applied as follows to confirm the paw withdrawal threshold: a less stiff fiber was applied; when no response was obtained, the next stiffest fiber in the series was applied to the same paw; if a response was obtained, a less stiff fiber was applied again. By using a data-fitting algorithm, the paw withdrawal threshold was calculated and subjected to parametric statistical analysis (13).

Heat sensitivity. Heat sensitivity was measured using the method described by Hargreaves and modified for mice (12, 14, 15). Mice were acclimated on a temperature controlled glass platform (23.5–24 °C) in the same plastic enclosures as the von Frey test. A radiant heat source and a timer were activated simultaneously with the heat source focused onto the mid plantar area of the hind paw. When the paw was withdrawn, both heat and timer were halted. Withdrawal latency of the paw from the heat source was measured. To prevent tissue damage, a 15-s cutoff was used. Three measurements were made per animal per test session.

BrdU Administration. To label proliferating cells, the thymidine analog BrdU (Sigma) was prepared in PBS and administered (50 mg/kg i.p.) once per day for 7 contiguous days or twice in 1 d with an 8-h interval. Animals were injected with BrdU 4 wk after irradiation and killed either 3 wk after the last BrdU injection of the 7-d protocol or 16 h after the second BrdU injection of the 1-d protocol (Fig. 2).

Tissue Processing. Mice were deeply anesthetized with ketamine and xylazine as described above and perfused intracardially with 0.9% NaCl. Brains were postfixed with 4% (wt/vol) PBS buffered paraformaldehyde for 48 h, and immersed in 30% (wt/vol) sucrose (in PBS) for cryoprotection. Forty-micrometer serial coronal sections encompassing the entire hippocampal formation were obtained with a sliding microtome (Leica SM 2000R, Leica). Free-floating brain sections were stored in 24-well plates at 4 °C in a cryoprotection solution containing 0.01 M NaH_2PO_4, 30% (vol/vol) glycerin, and 30% (vol/vol) ethylene glycol.

Immunohistochemical Staining. For the detection of BrdU, brain sections were washed in Tris-buffered Tween solution (TBST) and then treated with 0.6% hydrogen peroxide and 0.1% Triton X-100 at room temperature for 30 min. To denature DNA, sections were treated with 3 M hydrochloric acid (HCl) at 37 °C for 30 min. Sections were then incubated with a blocking solution containing 10% (vol/vol) rabbit serum in TBST for 1 h at room temperature, and then incubated with rat anti-BrdU (ab6326, 1:1,000 diluted in blocking solution; Abcam) overnight (about 16 h) followed by biotinylated secondary antibody (rabbit anti-rat IgG, BA-4000, 1:1,000; Vector Laboratories). For the detection of doublecortin (Dcx) and c-Fos, we omitted HCl treatment, and brain sections were incubated with goat anti-Dcx (sc-8066, 1:300; Santa Cruz Biotechnology) or rabbit anti–c-Fos (PC38, 1:20,000, EMD, Millipore) for 48 h at 4 °C followed by incubation with biotinylated secondary antibody at room temperature for 1 h. Sections were then treated with the ABC kit (PK-4000; Vector Laboratories), and diaminobenzidine (DAB, D5905; Sigma) was used to develop the signals. To determine the number of $BrdU^+/NeuN^+$ and $BrdU^+/GFAP^+$ cells in the subgranular zone (SGZ), immunofluorescence staining of BrdU/NeuN/GFAP was carried out. Brain sections were first rinsed in TBST and incubated in 3 M HCl to allow DNA denaturation. Sections were incubated simultaneously with rat anti-BrdU (1:1,000), mouse anti-NeuN (MAB377, 1:500; Chemicon), and rabbit anti-GFAP (Z0334, 1:1,000; Dako) in TBST containing 0.2% Triton X-100 (vol/vol) and 10% goat serum overnight (about 16 h) at 4 °C followed by incubation with secondary antibodies, Alexa 555 goat anti-rat IgG, Alexa 488 goat anti-mouse IgG, and Alexa 647 goat anti-rabbit IgG (all at 1:500 dilution; Invitrogen), at room temperature for 1 h. Sections were mounted with ProLong antifade (P36935; Invitrogen) solution and stored in −20 °C. One in every sixth sections of the entire hippocampal formation were used for BrdU staining and one in every 12th sections used for Dcx, c-Fos, and BrdU/NeuN/GFAP triple staining.

Cell Counting. The stereological counting principle of systematic, uniformly random sampling of sections (16) was applied to determine the total number of $BrdU^+$ and Dcx^+ cells in the SGZ, as well as c-Fos^+ cells in the granule cell layer, of hippocampal dentate gyrus. SGZ was defined as the ±16-μm zone along the border between the hilus and the granule cell layer. Any positively stained cells appearing at more than two times the nuclear diameter away from the border of granule cell layer were not considered. To avoid overestimation, only BrdU signals that can be identified as constituting the middle cross-section of a nucleus were counted. Spot-like patterns from small patches of chromatin/chromosome were not considered. The entire dentate gyrus (bilateral) of each brain section was photographed and the number of $BrdU^+$ cells in the SGZ was determined for each mouse. Total $BrdU^+$ cell counts were calculated by multiplying the initial counts by 6. Similar to BrdU analysis, Dcx^+ cells and Dcx^+ cells with a more mature appearance (i.e., category E and F Dcx^+ cells) (17) were counted in the SGZ. The total number of Dcx^+, mature Dcx^+ cells, and c-Fos^+ cells were calculated by multiplying the initial counts by 12.

Immunofluorescence stained sections were analyzed with a LSM 510 Confocal Laser Scanning Microscope (Carl Zeiss MicroImaging), with the detection pinhole set at 1 Airy Unit. *Z* sections were taken at 3-μm intervals. $BrdU^+$ cells were examined with split-panel analysis. Only those cells for which the $BrdU^+$ nucleus was unambiguously associated with the lineage-specific marker were scored as positive. For each lineage-specific marker, the percentage of $BrdU^+$ cells expressing that marker was determined. For most samples, at least 100 $BrdU^+$ cells were examined for lineage analysis. However, because KO mice had lower numbers of $BrdU^+$ cells, all $BrdU^+$ cells in every 12th sections were examined in the KO groups. Total number of lineage-specific $BrdU^+$ cells for each animal was then calculated by multiplying the percentage by the total number of $BrdU^+$ cells in the SGZ.

Activated Microglia. Total number of activated microglia was counted at the dorsal hippocampus level as described previously (18) with minor modifications. Rat anti-mouse CD68 monoclonal antibody (1:1,500, ab53444; Abcam) and biotinylated rabbit anti-rat IgG (1:200, BA-4001; Vector Laboratories) were used as the primary and secondary antibody, respectively. Staining signals were further amplified with an avidin/biotin amplification system (Vector Laboratories) followed by Cy3 tyramide amplification (PerkinElmer). Nuclei were counterstained with Cytox-Green (Invitrogen). Regions of interest containing the granular cell layer were selected using AxioImager imaging software (Zeiss) and the numbers of positive cells were counted within the selected area. To avoid overestimation, only intensely stained cell body with short, stout processes were counted. Eight coronally sectioned hippocampal dentate gyrus were examined for each mouse, and the final

results of activated microglia were expressed as number of cells per square millimeter.

Golgi Staining. A separate set of mice were used for Golgi staining and the procedure was carried out following behavioral studies. Golgi-Cox staining procedure was performed using the FD Rapid GolgiStain Kit (FD NeuroTechnologies). Coronal sections (100-μm thickness) were obtained with a Vibratome (VT1200S; Leica Microsystems) and were mounted on gelatin-coated slides. After color development, sections were examined with a Zeiss Imager D1 microscope, and images of dentate granular neurons were captured using an ORCA-ER digital camera (Hamamatsu Photonics). An investigator blinded to the genotype and treatment randomly selected dendrites (secondary and tertiary dendritic branches) from each mouse for quantification. Areas within 10 μm of the dendritic branch point or 10 μm of the dendritic terminals were excluded from analysis. Visible spines were counted in 10 dendritic segments (each 15–40 μm in length) from each mouse using ImageJ (National Institutes of Health). Only spines that were clearly protruding from the dendrites were counted, and they included two-headed, thin, and mushroom-shaped (19) spines. Spine density was expressed as average number of spines per 10-μm dendrite.

GFP Labeling of Newborn Neurons. GFP labeling of newborn neurons was carried out as described previously (20) using a retroviral vector MLV-CAG-GFP (21). High-titer MLV-CAG-GFP (1×10^8 units/mL) was injected stereotaxically into the dendate gyrus using the following coordinates: anterior-posterior (AP) = −2 mm from the bregma; lateral (LAT) = ± 1.6 mm; ventral (VENT) = 2.2 mm. Each site was injected with 0.5 μL retrovirus at a rate of 0.25 μL/min. Mice were killed 4 wk after injection to allow maturation of the newborn neurons. GFP-labeled cells were visualized with anti-GFP antibody (Invitrogen; A11122), and neurons were identified with NeuN antibody. The viral stock was produced by the Gene Vector and Virus Core facility at the Stanford Neuroscience Institute. Immunofluorescence stained sections were analyzed with a LSM 510 Confocal Laser Scanning Microscope (Carl Zeiss MicroImaging, Zeiss EC Plan-Neofluar, 20×/0.05) with the detection pinhole set at 1 Airy Unit. *Z* sections taken at 3-μm intervals were examined for GFP-labeled cells. The *z*-stack images of a single GFP^+ neuron were processed with ImageJ to obtain a stacked image. Dendrite tracing was then performed using the NeuronJ plugin. The traced images were used to determine the complexity of dendritic networks using the Advanced Sholl Analysis plugin. Dendritic lengths were obtained during the tracing process, and the number of branches was counted manually based on the traced image of GFP^+ neurons. Only GFP^+ cells with at least one dendrite (longer than the diameter of soma) were imaged and analyzed.

Western Blot Analyses. Protein levels of antioxidant enzymes, CuZn superoxide dismutase (CuZnSOD), Mn superoxide dismutase (MnSOD), EC-SOD, catalase, peroxiredoxin 1 (Prdx1), and peroxiredoxin 3 (Prdx3) in the hippocampus were determined by Western blot analysis using whole tissue homogenates. Fresh brains were dissected on ice and hippocampi were isolated, flash-frozen in liquid nitrogen, and stored at −80 °C. Hippocampal tissues from each animal were homogenized individually (weight to volume ratio 1:20) in T-PER buffer (Thermo Scientific), containing Complete protease inhibitor and phosphatase inhibitor (Roche). Homogenized samples were centrifuged at 10,000 × *g* at 4 °C for 5 min, and the supernatants were stored in 20-μL aliquots at −80 °C. Protein concentration of each sample was determined with a NanoVue spectrophotometer (GE Healthcare), and 50 μg of total proteins from each sample were used for Western blot analysis. Primary antibodies used in this study were described previously (18, 22). For quantification of the phosphorylated cAMP response element binding protein (pCREB, Ser133), nuclear extracts were used. Briefly, hippocampal tissues were treated with a hypotonic buffer (10 mM Hepes, 4 mM NaF, 10 μM Na_2MoO_4, 100 μM EDTA) to extract cytosolic proteins, followed by a nuclear extraction buffer [10 mM Hepes, 100 μM EDTA, 1.5 mM $MgCl_2$, 420 mM NaCl, 10% (vol/vol) glycerol, 1 mM DTT] to extract nuclear proteins. All buffers contained freshly prepared protease inhibitors and phosphatase inhibitors. Eighty micrograms of total nuclear proteins each were used for pCREB quantification (anti-pCREB, cat. No. 9198S, 1:1,000; Cell Signaling). IRDye-conjugated secondary antibodies were used for signal detection and quantification of all Western blot samples, and protein bands were visualized using an Odyssey Infrared Imaging System (Licor). Blots for antioxidant enzyme detections were reprobed with an antibody against β-actin (A3854, 1:50,000; Sigma) for normalization. pCREB signal intensities were normalized to the total DNA content of each sample.

Gene Expression Quantification by Quantitative PCR. Hippocampi were collected from individual mice, and RNA was extracted using TriZol reagent (Invitrogen) and reverse transcribed into cDNA using the SuperScript first strand synthesis kit (Invitrogen). Quantitative PCR (qPCR) was performed using the ABI 7900HT Sequence Detection System (Applied Biosystems) with SYBR Green PCR Master Mix (Applied Biosystems). Datapoints were calculated using standard curve methods and were expressed as the fold increase or decrease from the nonirradiated WT controls. The control value was set to 1.0, and GAPDH was used as an internal reference. Primers used for the qPCR analyses are listed in Table S2.

Statistical Analyses. Statistical analyses were carried out with GraphPad Prism 4.03 for Windows (GraphPad Software). One-way ANOVA with Tukey's posttest was carried out for comparison across multiple groups; two-way ANOVA with Bonferroni posttest was carried out to determine genotype × treatment interaction; and two-way repeated-measures ANOVA test was performed to compare the complexity of dendritic networks. Paired *t* test was carried out to compare results from RAWM (block 1 vs. block 10). Data tables for two-way ANOVA test were constructed in two different ways, with irradiation or genotype as the column factor, to allow postanalyses between 0 and 5 Gy within each genotype or analyses between WT, OE, and KO within each treatment group.

1. Zou Y, Chen CH, Fike JR, Huang TT (2009) A new mouse model for temporal- and tissue-specific control of extracellular superoxide dismutase. *Genesis* 47(3):142–154.
2. Carlsson LM, Jonsson J, Edlund T, Marklund SL (1995) Mice lacking extracellular superoxide dismutase are more sensitive to hyperoxia. *Proc Natl Acad Sci USA* 92(14): 6264–6268.
3. Mayford M, et al. (1996) Control of memory formation through regulated expression of a CaMKII transgene. *Science* 274(5293):1678–1683.
4. Acevedo SE, McGinnis G, Raber J (2008) Effects of 137Cs gamma irradiation on cognitive performance and measures of anxiety in Apoe-/- and wild-type female mice. *Radiat Res* 170(4):422–428.
5. Corniola R, Zou Y, Leu D, Fike JR, Huang TT (2012) Paradoxical relationship between Mn superoxide dismutase deficiency and radiation induced cognitive defects. *PLoS ONE* 7(11):e49367.
6. Mumby DG, Gaskin S, Glenn MJ, Schramek TE, Lehmann H (2002) Hippocampal damage and exploratory preferences in rats: memory for objects, places, and contexts. *Learn Mem* 9(2):49–57.
7. Shepherd JK, Grewal SS, Fletcher A, Bill DJ, Dourish CT (1994) Behavioural and pharmacological characterisation of the elevated "zero-maze" as an animal model of anxiety. *Psychopharmacology (Berl)* 116(1):56–64.
8. Alamed J, Wilcock DM, Diamond DM, Gordon MN, Morgan D (2006) Two-day radial-arm water maze learning and memory task; robust resolution of amyloid-related memory deficits in transgenic mice. *Nat Protoc* 1(4):1671–1679.
9. Villeda SA, et al. (2011) The ageing systemic milieu negatively regulates neurogenesis and cognitive function. *Nature* 477(7362):90–94.
10. Chaplan SR, Bach FW, Pogrel JW, Chung JM, Yaksh TL (1994) Quantitative assessment of tactile allodynia in the rat paw. *J Neurosci Methods* 53(1):55–63.

11. Sahbaie P, et al. (2009) Role of substance P signaling in enhanced nociceptive sensitization and local cytokine production after incision. *Pain* 145(3):341–349.
12. DeLorey TM, et al. (2011) Somatosensory and sensorimotor consequences associated with the heterozygous disruption of the autism candidate gene, Gabrb3. *Behav Brain Res* 216(1):36–45.
13. Poree LR, Guo TZ, Kingery WS, Maze M (1998) The analgesic potency of dexmedetomidine is enhanced after nerve injury: A possible role for peripheral alpha2-adrenoceptors. *Anesth Analg* 87(4):941–948.
14. Hargreaves K, Dubner R, Brown F, Flores C, Joris J (1988) A new and sensitive method for measuring thermal nociception in cutaneous hyperalgesia. *Pain* 32(1):77–88.
15. Li X, Angst MS, Clark JD (2001) A murine model of opioid-induced hyperalgesia. *Brain Res Mol Brain Res* 86(1-2):56–62.
16. West MJ (1999) Stereological methods for estimating the total number of neurons and synapses: Issues of precision and bias. *Trends Neurosci* 22(2):51–61.
17. Plümpe T, et al. (2006) Variability of doublecortin-associated dendrite maturation in adult hippocampal neurogenesis is independent of the regulation of precursor cell proliferation. *BMC Neurosci* 7:77.
18. Rola R, et al. (2007) Lack of extracellular superoxide dismutase (EC-SOD) in the microenvironment impacts radiation-induced changes in neurogenesis. *Free Radic Biol Med* 42(8):1133–1145, discussion 1131–1132.
19. Bourne JN, Harris KM (2008) Balancing structure and function at hippocampal dendritic spines. *Annu Rev Neurosci* 31:47–67.
20. Gu Y, Janoschka S, Ge S (2011) Studying the integration of adult-born neurons. *J Vis Exp*, (49):e2548.
21. Zhao C, Teng EM, Summers RG, Jr., Ming GL, Gage FH (2006) Distinct morphological stages of dentate granule neuron maturation in the adult mouse hippocampus. *J Neurosci* 26(1):3–11.
22. Kim A, et al. (2010) Enhanced expression of mitochondrial superoxide dismutase leads to prolonged in vivo cell cycle progression and up-regulation of mitochondrial thioredoxin. *Free Radic Biol Med* 48(11):1501–1512.

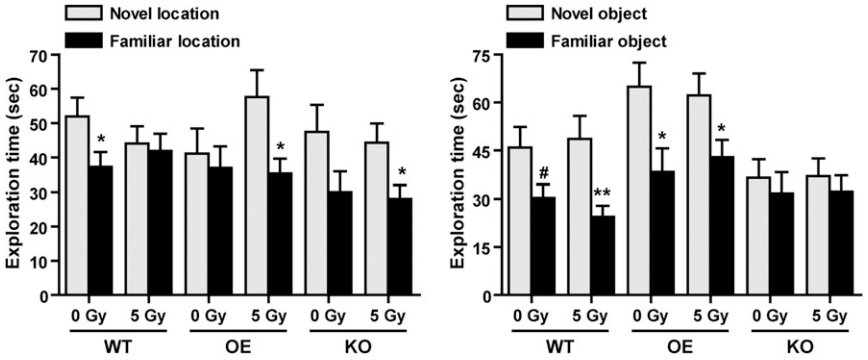

Fig. S1. Exploration time in NLR and NOR tests. Total exploration time (in seconds) was compared by Student *t* test between novel and familiar location/object within each cohort. $*P < 0.5$; $**P < 0.01$; $^{\#}P = 0.0533$. $n = 17–20$ mice per genotype per treatment.

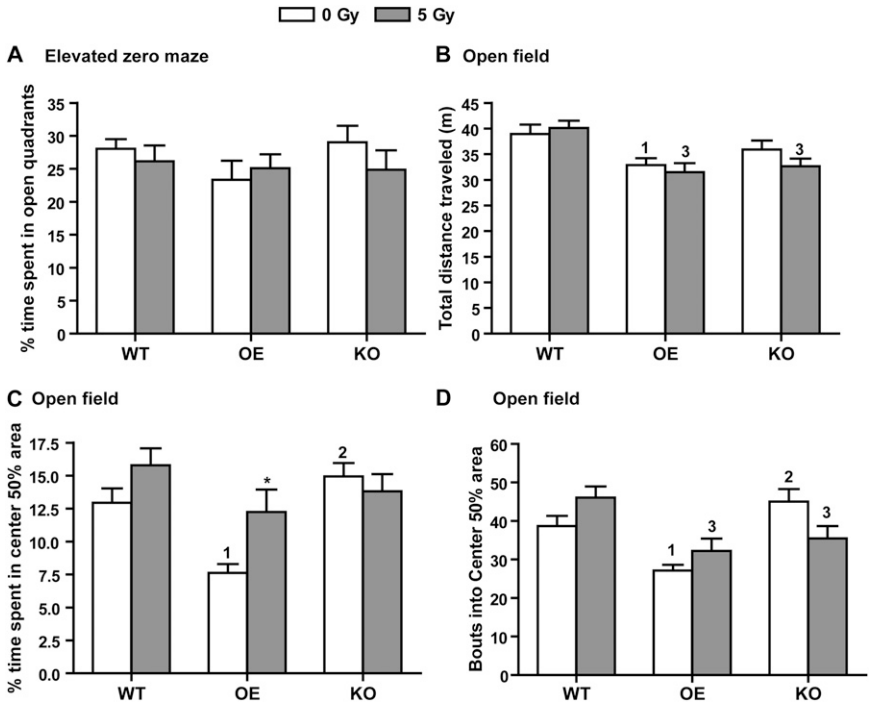

Fig. S2. Elevated zero maze and open field tests. (*A*) Results from elevated zero maze showing the average time spent in the two open quadrants during the 5-min testing period. (*B–D*) Results from open-field tests. (*B*) There was a small, but significant, reduction in total distance traveled in the open-field box in sham and irradiated OE mice. Irradiated KO mice also traveled a significantly shorter distance from irradiated WT controls. Only genotype [$F_{(2,106)} = 10.82$, $P < 0.0001$] contributed significantly to the data variation. (*C*) Sham-irradiated OE mice spent significantly less amount of time investigating the center 50% area of the open-field box. Irradiation [$F_{(1,106)} = 4.61$, $P = 0.0341$] and genotype [$F_{(2,106)} = 9.18$, $P = 0.0002$] both contributed significantly to the data variation. (*D*) Less time spent in the center 50% area in sham-irradiated OE mice was partly because of reduced entry into the open area. Bouts into the center 50% area in irradiated OE and KO mice were also significantly lower than that in irradiated WT mice. There was a significant interaction between treatment and genotype [$F_{(2,106)} = 5.23$, $P = 0.0068$]. Genotype [$F_{(2,106)} = 11.47$, $P < 0.0001$] also contributed significantly to the data variation. Data are presented as mean ± SEM. Two-way ANOVA with Bonferroni posttest was carried out. *$P < 0.05$ for comparison between 0 and 5 Gy within each genotype. 1, $P < 0.05$ compared with WT/0 Gy; 2, $P < 0.05$ compared with OE/0 Gy; 3, $P < 0.05$ compared with WT/5 Gy. n = 17–20 mice per genotype per treatment.

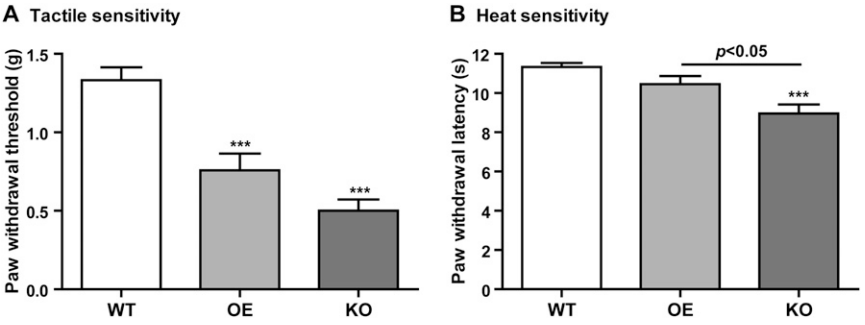

Fig. S3. Assessment of mechanical and heat sensitivity. Comparison of paw-withdrawal threshold after stimulation with von Frey filaments (*A*) and withdrawal latency to radiant heat (*B*). Data are presented as mean ± SEM and were analyzed by one-way ANOVA. Tactile sensitivity (*A*) $F_{(2,24)} = 23.4$, $P < 0.0001$; heat sensitivity (*B*), $F_{(2,24)} = 10.14$, $P = 0.0006$. Results from Bonferroni multiple comparison tests are presented on the bar graphs. ***$P < 0.001$ compared with WT mice. Data are presented as mean ± SEM. n = 9 mice each.

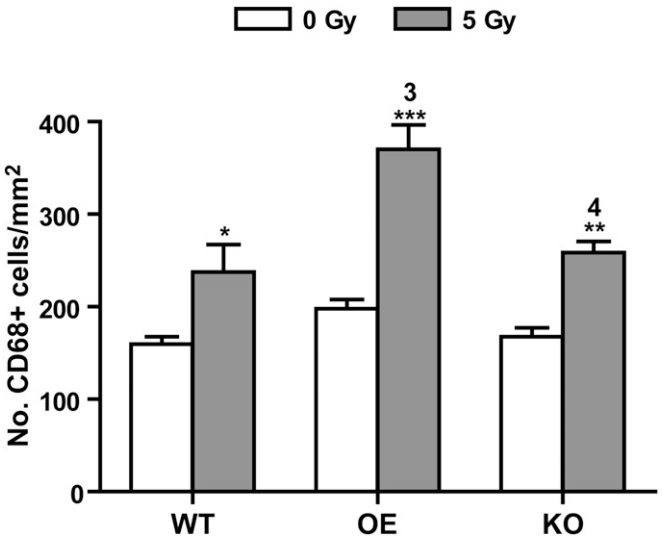

Fig. S4. Number of activated microglia in dorsal hippocampus. The number of $CD68^+$ cells in the hippocampal dentate gyrus was counted. Two-way ANOVA with Bonferroni posttest was carried out. Posttest results are presented on the graph: $*P < 0.05$, $**P < 0.01$, $***P < 0.001$ for comparison between 0 and 5 Gy within each genotype. 3, $P < 0.05$ compared with WT/5 Gy; 4, $P < 0.05$ compared with OE/5 Gy. There was a significant interaction between treatment and genotype [$F_{(2,24)} = 4.01$, $P = 0.0314$]. Irradiation [$F_{(1,24)} = 59.29$, $P < 0.0001$] and genotype [$F_{(2,24)} = 12.78$, $P = 0.0002$] also contributed significantly to the data variation. $n = 5$ mice per genotype per treatment. Data are presented as mean ± SEM.

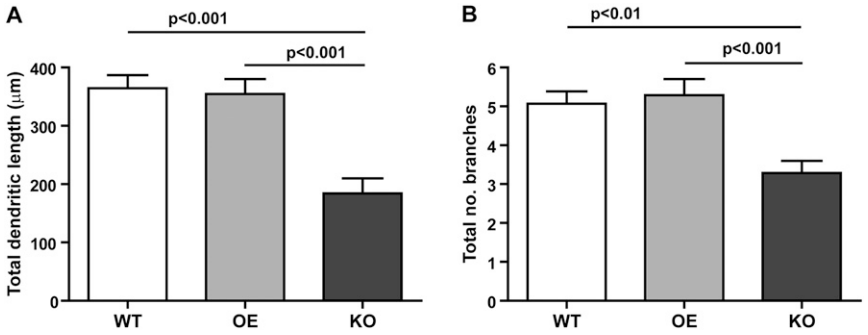

Fig. S5. Dendritic arborization of newborn neurons. Total dendritic length (*A*) and number of branches (*B*) were determined. Data were analyzed with one-way ANOVA with Tukey posttest. $n = 44$ (from three mice), 49 (from five mice), and 35 (from four mice) GFP^+ cells from WT, OE, and KO, respectively. Posttest results are shown on the graph. Data presented as mean ± SEM.

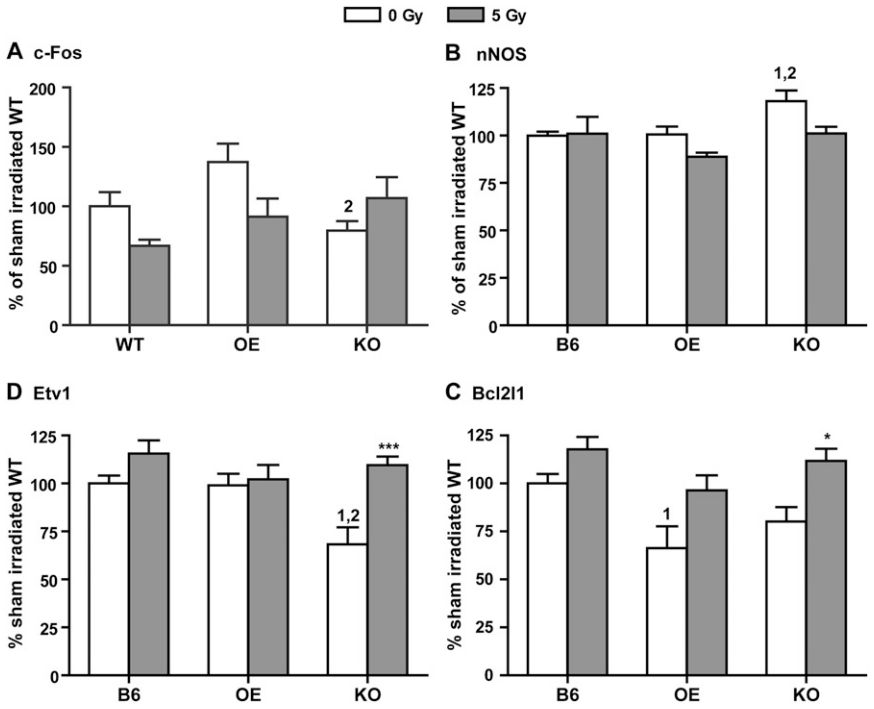

Fig. S6. Quantitative RT-PCR analyses of gene expression in the hippocampal formation. Expression levels of the immediate early gene c-Fos (*A*), neuronal-specific nitric oxide synthase (nNOS) (*B*), the transcription factor Etv1 (*C*), and the BCl2-like protein Bcl2l1 (*D*) were determined and compared between sham and irradiated WT, OE, and KO mice. All data (mean ± SEM) are compared with sham irradiated WT and expressed as percent sham-irradiated WT levels. Two-way ANOVA with Bonferroni posttest was carried out. $*P < 0.05$; $***P < 0.001$ for comparison between 0 and 5 Gy within each genotype. 1, $P < 0.05$ compared with sham irradiated WT; 2, $P < 0.05$ compared with sham irradiated OE mice.

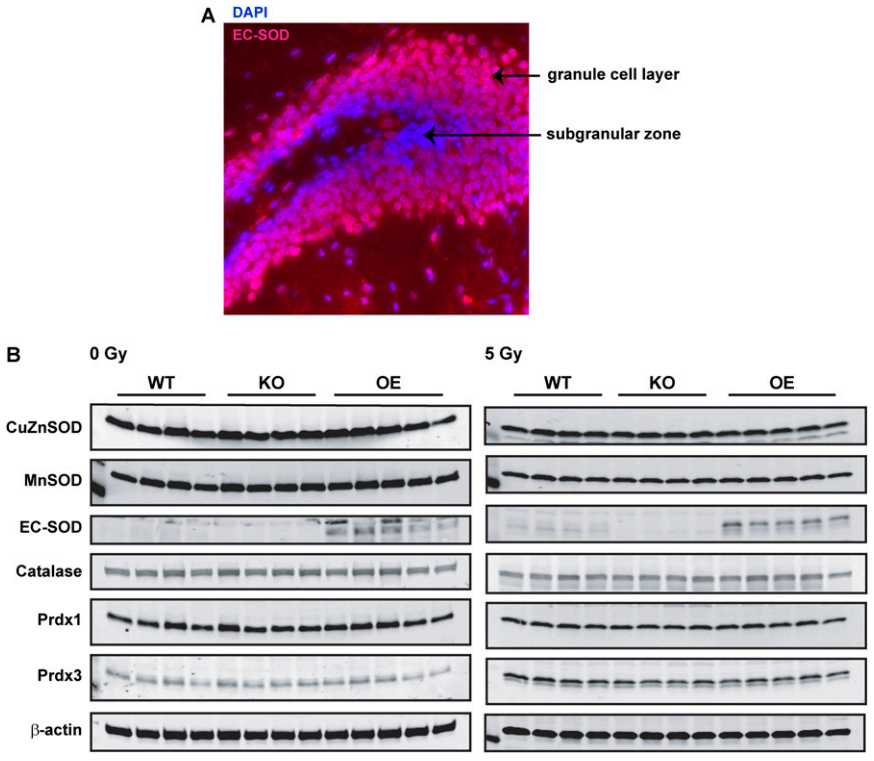

Fig. S7. Immuno-detection of EC-SOD and other antioxidant enzymes. (*A*) Immunohistochemical staining of EC-SOD in the dentate gyrus of OE mice. A representative picture showing EC-SOD stained in red with a rabbit polyclonal antibody and cell nuclei stained in blue with DAPI. A layer of blue cells in the SGZ indicates the EC-SOD–null status, and the red signals in granule cells indicate high levels of EC-SOD in this cell population. (*B*) Western blot analyses of tissue extracts from the hippocampal formation of sham and irradiated WT, OE, and KO mice. No overt changes in major antioxidant enzymes was observed in all experimental cohorts. Prdx1, peroxiredoxcin-1; Prdx3, peroxiredoxcin-3. β-actin was used as a loading control. $n = 4$, 4, and 5 for WT, KO, and OE, respectively.

Table S1. Summary of cell counts and percentage calculation

	WT		OE		KO	
Cells	0 Gy	5 Gy	0 Gy	5 Gy	0 Gy	5 Gy
$BrdU^+$ cells (short-term)	4,074 ± 131	2,538 ± 123	3,049 ± 372	2,310 ± 185	3,049 ± 128	2,657 ± 230
Dcx^+ cells	34,661 ± 1,191	20,568 ± 1448	22,894 ± 1,253	19,562 ± 1,593	17,350 ± 699	18,185 ± 1,992
Cat. E and F Dcx^+ cells	7,591 ± 626	7,331 ± 601	11,239 ± 476	10,114 ± 625	4,502 ± 584	6,790 ± 990
$BrdU^+$ cells (long-term)	2,560 ± 144	1,242 ± 42	1,870 ± 140	2,068 ± 111	734 ± 85	898 ± 101
Total $BrdU^+/NeuN^+$ cells	2,071 ± 124	721 ± 109	1,504 ± 130	1,790 ± 102	535 ± 92	548 ± 95
$BrdU^+/NeuN^+$ cells (as % $BrdU^+$)	80.9 ± 1.7%	67.7 ± 2.5%	87.2 ± 1.9%	83.3 ± 2.8%	81.3 ± 4.1%	61.5 ± 4.7%
Total $BrdU^+/GFAP^+$ cells	310 ± 33	251 ± 38	141 ± 27	229 ± 52	92 ± 22	230 ± 32
$BrdU^+/GFAP^+$ cells (as % $BrdU^+$)	12.2 ± 1.3%	23.7 ± 0.8%	8.0 ± 1.3%	10.4 ± 2.2%	14.9 ± 3.6%	30.0 ± 4.9%
Spine density (per 10 μm)	12.91 ± 0.55	9.81 ± 0.98	10.88 ± 0.48	12.67 ± 0.68	12.14 ± 0.73	11.43 ± 0.93
c-Fos^+ cells	643 ± 114	449 ± 106	1234 ± 129	942 ± 117	791 ± 201	338 ± 94
$BrdU^+/NeuN^+$ (as % Dcx^+ cells)	6.0%	3.5%	6.6%	9.2%	3.1%	3.0%

Table S2. Primers used for quantitative RT-PCR analyses

Gene	Forward primer	Reverse primer
Bcl2l1	5′-GGG ATG GAG TAA ACT GGG GTC-3′	5′-TGT TCC CGT AGA GAT CCA CAA A-3′
Bdnf	5′-TCA TAC TTC GGT TGC ATG AAG G-3′	5′-AGA CCT CTC GAA CCT GCC C-3′
Efna5	5′-ATT CCA GAG GGG TGA CTA CCA-3′	5′-GTG AGG GCA GAA AAC ATC CAG-3′
Etv1	5′-GCA AGT GCC TTA CGT GGT CA-3′	5′-CTT CAG CAA GCC ATG TTT CTT-3′
Fos	5′-CGG GTT TCA ACG CCG ACT A-3′	5′-TTG TCA CTA GAG ACG GAC AGA-3′
GAPDH	5′-TGG CAA AGT GGA GAT TGT TGC C-3′	5′-AAG ATG GTG ATG GGC TTC CCG-3′
nNOS	5′-CTG GTG AAG GAA CGG GTC AG-3′	5′-CCG ATC ATT GAC GGC GAG AAT-3′
Nr4a2	5′-GTG TTC AGG CGC AGT ATG G-3′	5′-TGG CAG TAA TTT CAG TGT TGG T-3′
Ntf3	5′-GGA GTT TGC CGG AAG ACT CTC-3′	5′-GGG TGC TCT GGT AAT TTT CCT TA-3′
Sema 3C	5′-CAA AAT GGC TGG CAA AGA TCC-3′	5′-TCC CCG GTT CAG GTA GGT G-3′